Frontiers in Computing and Intelligent Systems
ISSN: 2832-6024 | Vol. 15, No. 1, 2026

Six-Phase Worm Drive Motor Design with Fault – Tolerant Control

Chenyi Dong [1], Changlin Song [1, *], Chengjiao Ma [1], Junmin Li [1], Ju Long [2]

[1] School of Mechanical Engineering, Xihua University, Chengdu, Sichuan 610039, China
[2] School of Energy and Power Engineering, Xihua University, Chengdu, Sichuan 610039, China

[*] **Corresponding author**: Changlin Song (Email: 0120100007@mail.xhu.edu.cn)

Abstract: With the continuous development of industrial technology, multi-phase motors are widely used in fields such as industrial robots, ships, and automobiles. The performance requirements for motors are increasing, making their integration and reliability particularly important. To address the issues of low integration and the need for additional braking devices in traditional externally-driven reducers, this paper designs a six-phase fault-tolerant motor based on a built-in drum-shaped worm reducer, integrating worm drive with the six-phase fault-tolerant motor to achieve drive, control, and transmission as a unified system. This study focuses on the fault-tolerant control strategies for a six-phase permanent magnet synchronous motor (PMSM) under a single-phase open-circuit fault. Based on the principle of constant total magnetomotive force, two fault-tolerant control methods: minimum current and maximum output torque are proposed. The effectiveness and stability of these strategies in maintaining stable operation under rated load after a phase-loss fault are verified through MATLAB/Simulink simulations and prototype experiments.

Keywords: Six-phase Fault-tolerant Motor; Permanent Magnet Synchronous Motor; Fault-tolerant Control Method.

1. Introduction

Research on fault-tolerant control of six-phase motors can be traced back to the 1950s, with preliminary studies on multi-phase motors. In 1959, D.C. White and H.H. Woodson conducted an in-depth exploration of electromechanical energy conversion, particularly focusing on the energy conversion relationships in multi-phase motors. Their work initially revealed the relevant laws governing energy conversion in multi-phase motors of any phase configuration [1]. In 1995, Zhao Y and Lipo T.A. innovatively applied the vector space decomposition method to implement space vector PWM control. They detailed the related control principles, algorithm derivations, and implementation methods, demonstrating through theoretical analysis and experimental validation the advantages of this control strategy in improving torque performance, enhancing operational efficiency, and strengthening dynamic response in dual three-phase induction motors [2]. Federico Barrero from the University of Seville and Mario J. Duran from the University of Malaga conducted research targeting five-phase and asymmetrical six-phase induction motors. They proposed phase-loss fault-tolerant methods based on model predictive current control, pulse-width modulation techniques based on inverter switching frequency control, and flux adaptation methods to improve post-fault motor performance. Their work provided support and ideas for the development of multi-phase motor technology, promoting its application across various fields [3-6].

This paper combines the advantages of planar-tooth internal gear enveloping drum worm drives and multi-phase motors, cleverly integrating a six-phase motor with a worm gear. A six-phase external rotor worm motor is designed and manufactured, and its fault-tolerant control strategies are investigated. The prototype is then applied to a motor-driven worm gear reducer, and fault-tolerant control verification under motor operation is conducted, ultimately achieving stable operation of the reducer. This six-phase worm gear reducer is primarily suitable for industrial robotic arms and humanoid robots.

2. Structural Composition of the Reducer Motor

Currently, the reducers used in industrial robot joints domestically and internationally are mainly divided into two categories: harmonic reducers and RV reducers. Some special-purpose robots employ worm gear reducers. However, all these reducers have certain limitations. This paper proposes a novel worm drive structure that adopts a highly integrated design combining drive, control, transmission, and support into a unified system. In terms of drive, an external rotor worm motor is utilized to achieve driving, making full use of the internal space of the worm. For control, the worm motor employs closed-loop control through feedback of angular displacement and angular velocity signals from the motion output end, resulting in a simple control method with stable performance. Regarding transmission, the reducer adopts an adjustable-backlash internal meshing planar enveloping drum worm drive. This transmission method offers advantages such as a high transmission ratio, compact structure, small size, strong load-bearing capacity, high transmission accuracy, grindable tooth surfaces, long service life, and ease of achieving mechanical self-locking. In terms of support, the structure is supported via support shafts and their shaft systems, while sealing is achieved through a cylindrical structure formed by the worm wheel and worm wheel seat. This support method eliminates the need for a complex housing, making the structure simple, compact, and easy to manufacture.

As shown in Figure 1, the three-dimensional model of the worm gear reducer illustrates that a bracket is assembled and fixed onto the worm wheel shaft, thereby providing assembly support for the worm motor. The shafts of the two worm motors are assembled with the bracket. After fixation, the worm meshes with the worm wheel, and finally, end covers are installed to complete the assembly. The reducer is driven by two external rotor motors, transmitting motion from the inside outward, and adopts a worm-and-wheel structure. When power is cut off, the reducer features a self-locking protection function, where the output end immediately maintains its stopped position without the need for additional braking devices as required in traditional robot joint reducers.

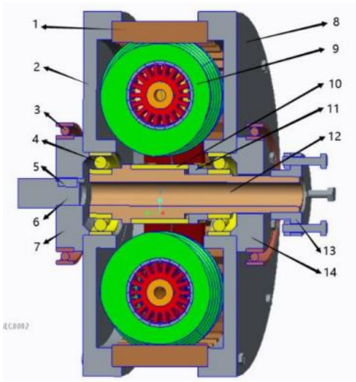

1.Worm wheel 2. First worm wheel housing 3. Bearing 4. Deep groove ball bearing 5. Key 6. Connecting shaft 7. End cover 8.Second worm wheel housing 9. Worm (motor rotor) 10. First bracket 11. Sleeve 12. Worm wheel shaft 13. Flange 14. Second end cover

Figure 1. Worm gear reducer 3D model

Table 1. Key parameters of the reducer

Order number	Parameter	Value
1	Worm start Z1	1
2	Worm gear teeth number Z2	50
3	Module M1	4
4	Helix direction	right

2.1. Working Principle of the Reducer Motor

The worm is a single-start worm. The worm bracket is assembled and fixed to the reducer shaft and remains stationary, while the motor stator shaft is fixedly assembled to the bracket. The interior of the worm is designed as a six-phase external rotor motor. After the motor is energized, the worm rotor rotates, thereby driving the worm wheel to complete the transmission. The worm-shaped external rotor motor belongs to the category of brushless DC motors, and its three-dimensional assembly structure is shown in Figure 2. The structural composition of this motor is as follows: first, the 1-worm bracket provides stable support for the motor assembly; next, the 2-stator shaft, as one of the core components, carries key components such as the stator windings; the 3-end cover and 7-end cover, along with the other end cover 9, are distributed on both sides of the motor, serving to enclose and protect the internal structure while assisting in positioning; the 4-bearing and 6-bearing are used to achieve a smooth connection between the stator shaft and the external rotor worm, ensuring flexible relative rotation, while relying on shaft shoulders and shaft rings for precise positioning to guarantee assembly accuracy; the 5-external rotor worm is a highly distinctive and critical part of this motor. Its feature lies in directly designing and manufacturing the worm as the external rotor of the motor, giving the motor an overall worm shape. In this way, the torque generated during motor operation can act directly on the worm wheel, greatly simplifying the number of transmission stages and effectively avoiding the cumulative layering of transmission errors; the 8-worm bracket is equally indispensable, contributing to the stable assembly of the motor.

The assembly scheme follows a rigorous design logic: the interior of the external rotor worm is hollow to precisely accommodate the stator shaft, installation of permanent magnets, etc., creating conditions for a compact internal structural layout; the permanent magnets are firmly attached to the inner wall of the worm-shaped external rotor through an adhesive process, providing a stable magnetic field source for the motor; the stator shaft is flexibly connected to the external rotor worm via bearings, with the bearings positioned accurately by carefully designed shaft shoulders and shaft rings. The end covers on both sides further tightly connect and precisely position the bearings and the worm, establishing a stable rotational system; one side of the stator shaft is seamlessly connected to the bracket via an end cover, while the other side achieves connection through precise coordination with the support plate. Furthermore, a hole is deliberately opened on the right side of the shaft to reserve appropriate space for the routing and installation of various wires and other related components, thereby ensuring that the entire motor assembly is structurally complete, operates reliably, and meets practical application requirements.

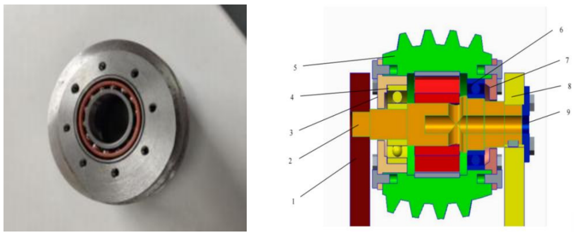

(a) Physical photograph (b) 3D cross-sectional view

Figure 2. Motor structure

2.2. Vector Control of Six-Phase PMSM

The VSD coordinate transformation treats the six-phase PMSM as a whole. The performance of this control method heavily relies on the accuracy of motor parameters, such as stator resistance and inductance. During operation, these parameters may change due to factors like temperature variations and magnetic circuit saturation, thereby affecting control effectiveness. Therefore, this section proposes vector control based on the double d-q coordinate transformation. This method decomposes the variables of the multi-phase motor into two synchronous rotating coordinate systems (dual d-q axes) for control. It views the six-phase PMSM as two three-phase subsystems and then applies the traditional three-phase motor coordinate transformation to control each subsystem separately. This approach can better achieve motor decoupling and improve motor performance. For example, in a six-phase motor, it can reduce harmonic content, lower torque ripple, and enhance motor efficiency and reliability.

Figure 3 shows the block diagram of vector control based on the double d-q coordinate transformation. This method is entirely equivalent to controlling two three-phase PMSMs, with both three-phase systems employing the ($i_d = 0$) control strategy.

As shown in Figure 3, the q-axis reference currents (i_q) for the two independent winding sets are identical, both being the output of the speed loop regulator. When the d-axis current inputs are set as ($i_{d1} = i_{d2} = 0$), according to the electromagnetic torque equation derived from the mathematical model of the six-phase PMSM under the double d-q coordinate transformation in the rotating coordinate system, as long as the value of (i_{q1}+ i_{q2}) remains unchanged, the output electromagnetic torque does not vary. Since (i_{q1}= i_{q2}) ensures that the currents output by the two independent winding sets are sinusoidal with equal amplitudes, it further guarantees that both independent winding sets can deliver equal power. Therefore, this scheme represents an optimal solution.

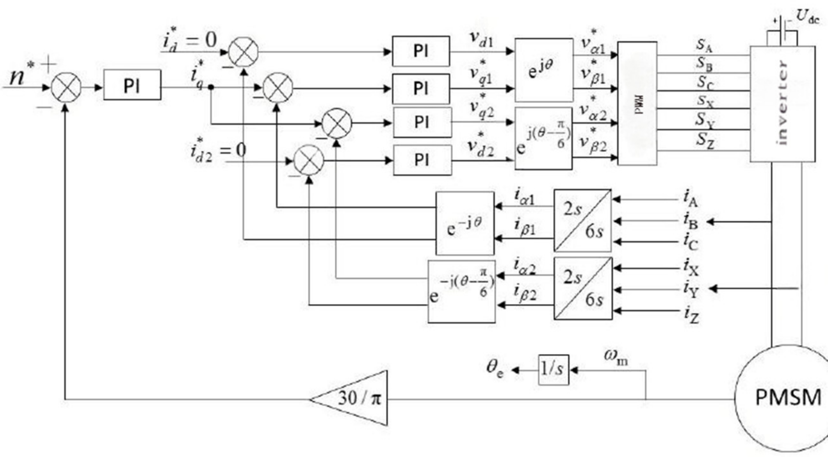

Figure 3. Vector control based on double D-Q coordinate transformation

2.3. Vector Control Model Simulation

Based on the results of the motor's physical design, the motor parameters required for the simulation process are listed in a table, as shown in Table 2.

Figure 4 shows the control system model of the six-phase PMSM based on the double d-q coordinate transformation. In the figure, (a) represents the PI controllers for the speed loop and current loop, along with the SVPWM calculation module under the double d-q coordinate transformation for the six-phase PMSM, while (b) depicts the six-phase inverter module.

Table 2. Six-phase PMSM simulation related parameters

Parameter	Value	Parameter	Value
Number of pole pairs	13	Stator inductance	0.33e-3mH
Winding resistance	1.46 Ω	Stator inductance	0.33e-3mH
d-axis main inductance	0.2e-3 mH	Leakage inductance	0.25e-3mH
q-axis main inductance	0.2e-3 mH	Flux linkage	0.0036 Wb
Moment of inertia	2.8e-5Kg ·m2	DC bus voltage	24 V

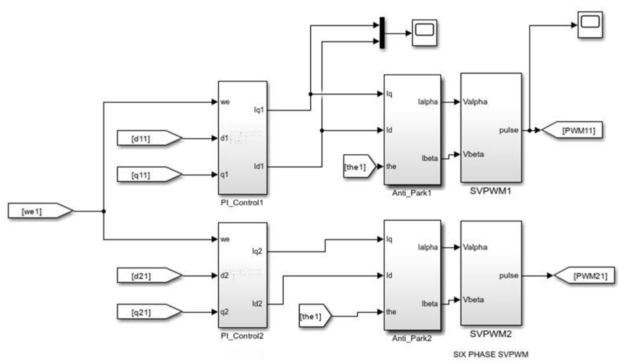

(a) Six-phase PI controller and SVPWM model

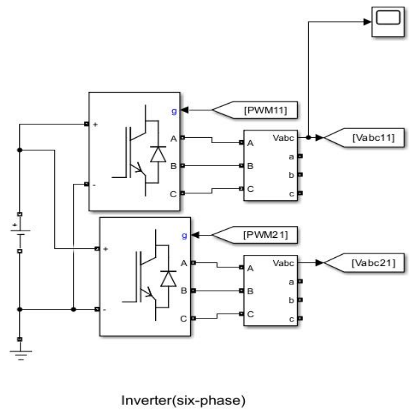

(b) Six-phase inverter model

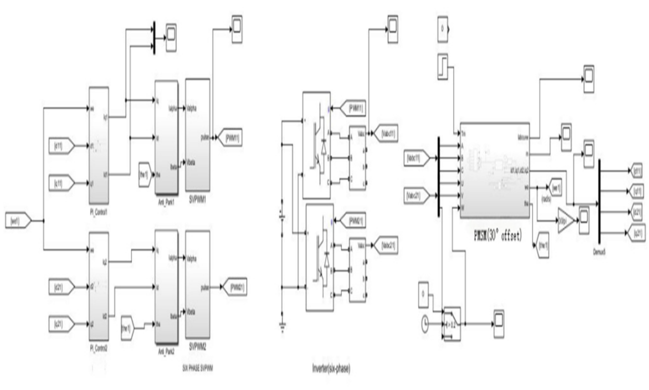

(c) Six-phase PMSM control system

Figure 4. A six-phase PMSM control system model based on double d-q coordinate transformation

2.4. Minimum-Current Fault-Tolerant Control for Single-Phase Open Circuit

The fundamental magnetomotive force exhibits a cosine distribution in space, with its amplitude varying over time according to the current variation pattern (cos(ωt)). Thus, the fundamental magnetomotive force is both a spatial function and a temporal function. Figure 5 shows the simulation model of the minimum current fault-tolerant control system for a six-phase PMSM under a single-phase open-circuit condition, which is based on the principle of constant total magnetomotive force and employs a hysteresis-controlled double d-q transformation model. At 0.2 s, the Switch module in Matlab/Simulink is used to disconnect one phase (phase F) of the normally closed-loop operating six-phase PMSM, simulating an open-circuit winding condition. Simultaneously, this module switches the normal control strategy to the fault-tolerant control based on the principle of constant total magnetomotive force. The motor speed is set to the rated speed of 1600 r/min, the motor load is 0.3 N·m, and the simulation duration is 0.5 s.

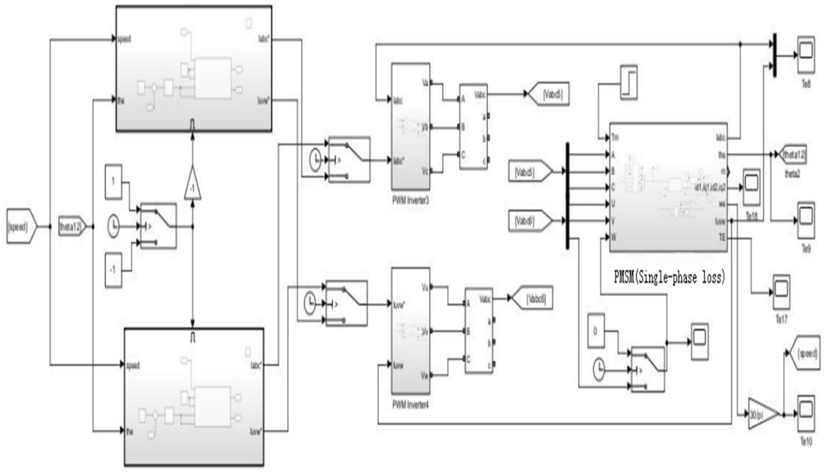

Figure 5. Simulation model of minimum current fault-tolerant control based on the principle of constant total magnetomotive force

Based on the motor design scheme in this paper, the load line current density selected during motor design is 26.83 A/mm², which is relatively high. Therefore, when a motor phase-loss fault occurs, special attention must be paid to ensuring that the current amplitudes in the remaining healthy phases are not excessive, to prevent overcurrent damage to the winding coils. Consequently, an objective function f for minimizing current during phase loss needs to be formulated and solved.

When a six-phase PMSM experiences a phase-disconnection fault and fault-tolerant control is implemented using the minimum current approach, the following scenario occurs: the current amplitude in motor phase A is smaller compared to the other phases, with phases B and C having equal current amplitudes, and phases D and E also having equal current amplitudes. Additionally, phases A and D share the same phase angle. This control method reduces the stress on the inverter capacity and effectively prevents further faults, although the losses in each phase differ. Figure 6 shows the vector distribution diagram of the phase currents.

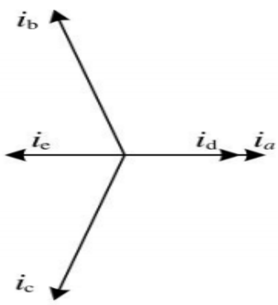

Figure 6. Vector diagram of the residual phase currents in the minimum current model.

2.5. Maximum Output Torque Fault-Tolerant Control Under Single-Phase Open-Circuit Condition

Figure 7 illustrates the simulation model of the maximum output torque fault-tolerant control system for a six-phase PMSM under a single-phase open-circuit condition, based on the principle of constant total magnetomotive force and employing a hysteresis-controlled double d-q transformation model. At 0.2 s, the Switch module in Matlab/Simulink is utilized to disconnect one phase (phase F) of the normally closed-loop operating six-phase PMSM, simulating an open-circuit winding condition. Simultaneously, this module switches the normal control strategy to the fault-tolerant control based on the principle of constant total magnetomotive force. The motor speed is set to the rated speed of 1600 r/min, the motor load is 0.3 N·m, and the simulation duration is 0.5 s.

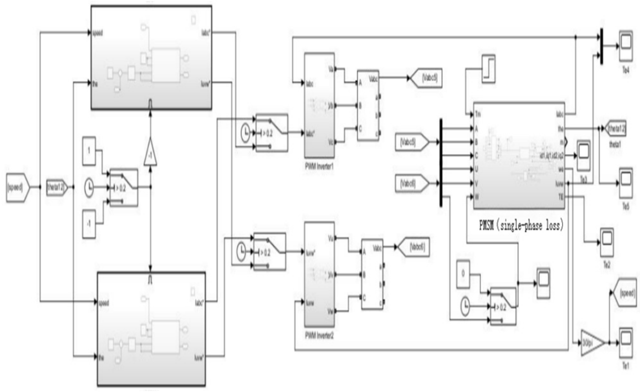

Figure 7. Simulation model of maximum output torque fault-tolerant control based on the principle of constant total magnetomotive force.

When maximizing output torque is set as the current optimization objective, among the remaining five-phase currents after a fault occurs, only phases B, C, D, and E are required to output current. The phase angles between these four currents are all 90°, and their amplitudes remain balanced. In this way, the motor can achieve fault-tolerant operation, effectively avoiding damage caused by excessive losses in any single phase and ensuring stable motor operation under special working conditions. At the same time, it can be observed that after phase F becomes open-circuited, the re-planned current results in phase A current being zero, which is also suitable for scenarios where both phases A and F are simultaneously open-circuited. Figure 8 shows the vector diagram of the residual phase currents under maximum output torque operation.

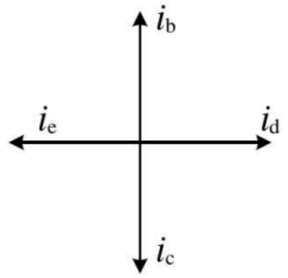

Figure 8. Vector diagram of the residual phase currents in the maximum output torque model.

3. Experiment and Analysis

3.1. Minimum-Current Fault-Tolerant Control for Single-Phase Open Circuit

In Figure 9 (a), the variation curve of the motor's mechanical angular velocity ω_e over time is shown. It can be observed from the figure that under this control mode, the motor responds rapidly and operates at a steady speed. When a load is suddenly applied at 0.2 seconds, the motor speed drops sharply but is quickly "corrected" under the regulation of the PI controller and then maintains constant-speed operation. Figure 9 (b) displays the variation curve of the electromagnetic torque T_e over time, indicating that at 0.2 seconds, the motor torque rapidly reaches 0.3 N·m, corresponding to the speed fluctuation. Figure 9 (c) shows the variation curves of the phase-A current i_a and phase-D current i_d over time. During the period from 0 to 0.2 seconds, the motor operates under no-load conditions with small current; at 0.2 seconds, the current increases abruptly due to the sudden load application, reaching an amplitude of 2.16 A, which matches the current excitation in the motor's finite element simulation. From 0.2 to 0.5 seconds, the motor operates under rated load, and it can be seen in the figure that there is a 30-degree phase difference between the phase-A current i_a and the phase-D current i_d. Figure 9 (d) illustrates the variation curves of the d-q axis currents over time. In the control strategy of this paper, the d-axis current is maintained at zero. At 0.2 seconds, the q-axis current increases and then remains stable.

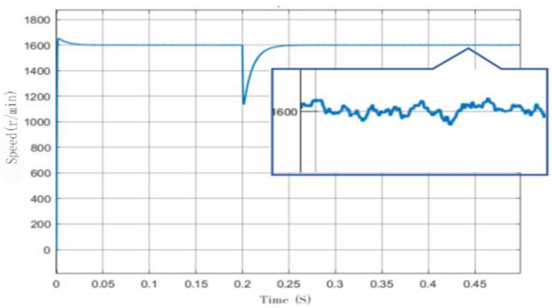

(a) Variation curve of mechanical angular velocity ω_e

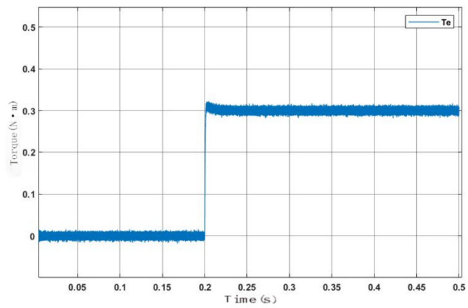

(b) Variation curve of electromagnetic torque T_e

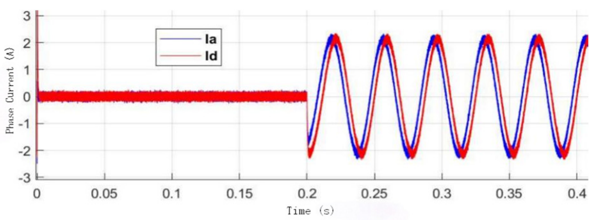

(c) Variation curves of phase currents i_a and i_d

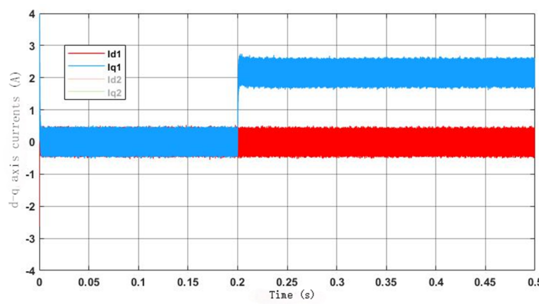

(d) Variation curves of d-q axis currents

Figure 9. Simulation results of six-phase PMSM vector control based on double d-q coordinate transformation

It can be seen from the figure that during motor startup, the speed curve based on the double d-q coordinate transformation model has an overshoot of approximately 0.31%, but the system response under this control is relatively sluggish. After a sudden load is applied at 0.2 seconds, the speed regulation by the controller becomes pronounced. The speed recovery time under the double d-q coordinate transformation model is about 0.05 seconds, which improves the response time by approximately 41.6% compared to the VSD coordinate transformation model.

3.2. Minimum-Current Fault-Tolerant Control for Single-Phase Open Circuit

As shown in Figure 10, before the disconnection of the F-phase winding at 0.2 seconds, all six-phase current waveforms are symmetrical, with the two winding sets having a 30° phase difference between them and a phase current amplitude of 2.16 A. At 0.2 seconds, the F-phase winding is disconnected and fault-tolerant control is activated. At this point, the motor phase currents fluctuate but quickly stabilize to operate according to the reference current (minimum copper loss current) under the fault-tolerant control strategy. It can be observed from the figure that after fault tolerance is applied, the currents in phases B and C have different phases but the same amplitude of 3.85 A, which is 1.782 times the normal current. The currents in phases D and E have opposite phases with the same amplitude of 1.80 A, which is 0.833 times the normal current. The current amplitude in phase D is 1.807 A, which is 0.833 times the normal current, and its phase is the same as before.

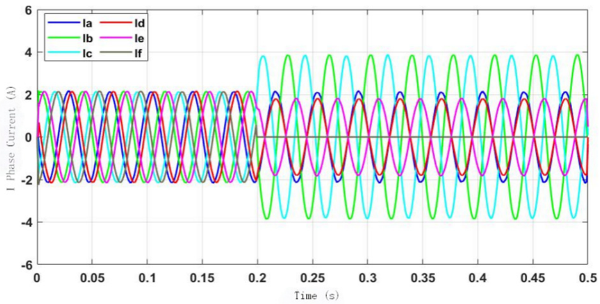

Figure 10. Current waveform of the minimum current fault-tolerant control strategy.

According to theoretical calculations, the current amplitudes of phases B and C should be 1.803 times the normal current, resulting in a simulation deviation of 0.07 A. The amplitudes of phases A and D should be 0.866 times the normal current, with a simulation deviation of 0.04 A. The analysis indicates that the cause of this error is suboptimal tuning of the current loop parameters in the PI controller.

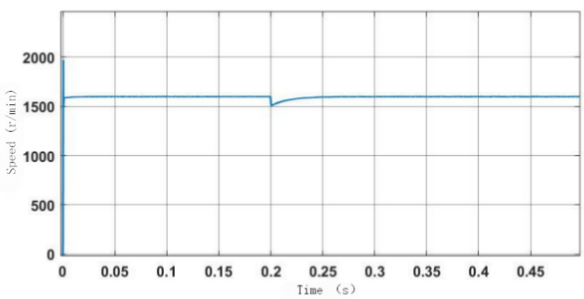

Figure 11. Speed waveform of the minimum current fault-tolerant control strategy.

As shown in Figure 11, the motor reaches the rated speed of 1600 r/min within an extremely short time during startup, exhibiting a certain overshoot but stabilizing quickly. At 0.2 s, when the F-phase of the motor is disconnected, the motor speed drops by nearly 100 r/min. The fault-tolerant control responds instantly upon phase loss, and it can be observed that the motor speed rapidly recovers within 0.04 s and stabilizes at the rated speed for steady operation.

As shown in Figure, the load torque waveform under the minimum current fault-tolerant control strategy is presented. The rated load torque of the motor is 0.3 N·m. Before 0.2 s, the motor operates normally, with the average and effective values of the load torque being 0.3 N·m, a maximum of 0.311 N·m, a minimum of 0.287 N·m, and a maximum load torque fluctuation of 8%. After 0.2 s, when the F-phase of the motor is open-circuited, fault-tolerant control is activated. The average and effective values of the fault-tolerant torque are 0.299 N·m, with a maximum of 0.325 N·m, a minimum of 0.273 N·m, and a maximum load torque fluctuation of 17%. The primary reason for the relatively large torque fluctuation is that the parameters of the current loop PI controller in this model require further adjustment.

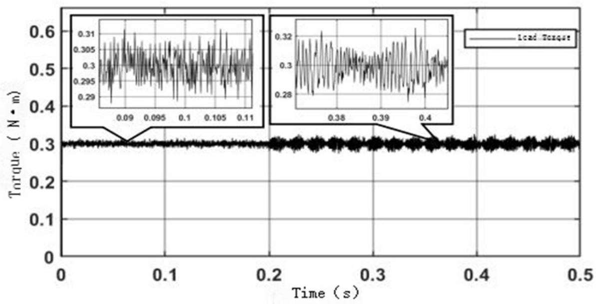

Figure 12. Torque waveform of the minimum current fault-tolerant control strategy.

3.3. Results of Maximum Output Torque Fault-Tolerant Control Strategy

At 0.2 s, when the F-phase is disconnected, the current undergoes a sudden change. Under the regulation of the fault-tolerant control strategy, the output current of phase A becomes zero, leaving only the remaining four phases operational. As shown in Figure 13, after fault tolerance is applied, the amplitudes of the remaining four-phase currents are equal, all at 3.75 A, which is 1.736 times the normal current—almost identical to the theoretical calculation of 1.732 times. The phase angles between the currents differ by 90 degrees, consistent with the theoretical calculations.

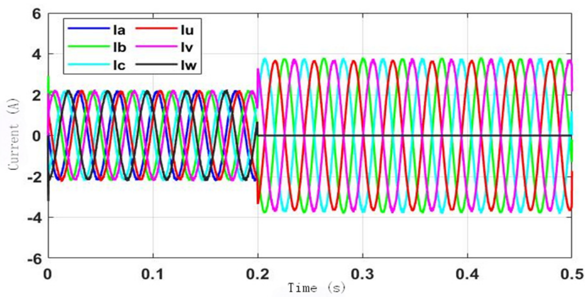

Figure 13. Current waveform of the maximum output torque fault-tolerant control strategy.

As shown in Figure 14 and Figure 15, the motor speed and torque waveforms under the maximum output torque fault-tolerant control strategy are presented. Before 0.2 s, the motor operates normally, responding quickly during startup and stabilizing at the rated speed of 1600 r/min within an extremely short time. At 0.2s, when the F-phase is disconnected, the motor speed drops abruptly. Under the regulation of the fault-tolerant control strategy, the motor speed decreases by approximately 50 r/min, which is about 50% of the speed drop in the minimum current model, and then rapidly recovers to the rated speed within 0.01s for stable operation. Before 0.2s, the motor operates normally. After 0.2s, when the F-phase of the motor is open-circuited, fault-tolerant control is activated. The average and effective values of the fault-tolerant torque are 0.300 N·m, with a maximum of 0.325 N·m, a minimum of 0.274 N·m, and a maximum load torque fluctuation of 17%.

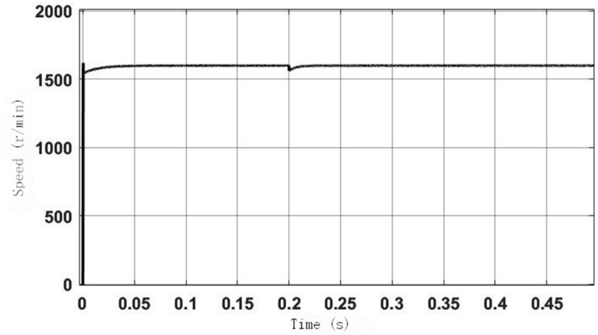

Figure 14. Speed of the maximum output torque fault-tolerant control strategy.

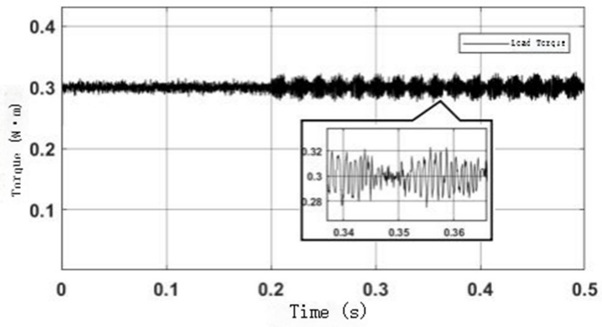

Figure 15. Torque of the maximum output torque fault-tolerant control strategy.

3.4. Prototype Performance Data

After the motor clamping is completed, the dynamometer platform is used for automatic mode testing. The motor characteristic curves are shown in Figure 16:

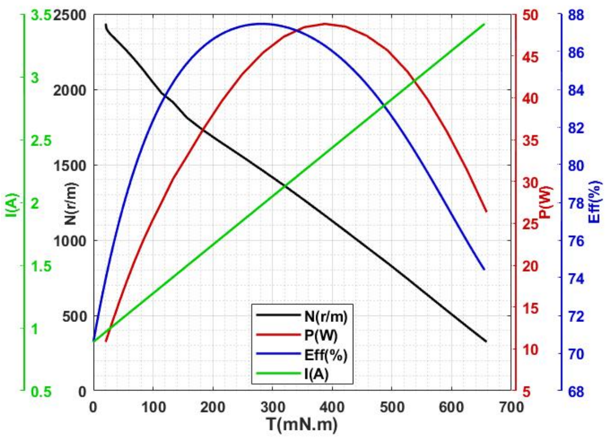

Figure 16. Characteristic curve of the six-phase worm motor.

The motor has a rated voltage of 24 V, a rated phase current of 2.1 A, and a rated power of 50.2 W. The figure shows that the rated power is slightly lower than the simulated power of 50.2 W. Analysis suggests that the cause of this deviation is windage and friction losses in the motor. The test results indicate that as torque increases, the motor speed tends to decrease, while the output power first rises and then declines. The highest efficiency is approximately 87%. At the no-load point, the torque is 0.01 N·m, and the speed is 2415 r/min. The maximum torque reaches 657.8 mN·m. At the rated operating point (300 mN·m, 1600 r/min), the efficiency of the six-phase motor is approximately 85%.

4. Conclusion

This study integrates the worm gear with a six-phase fault-tolerant motor, combining drive, control, and transmission into a single unit. This design results in a compact reducer structure. By adopting a worm gear mechanism as the robot joint reducer, mechanical self-locking and braking are structurally achieved. The use of a six-phase motor ensures that the joint reducer can continue to operate under load even in the event of a phase-loss fault (inverter or winding failure), effectively enhancing the safety and reliability of the system.

References

[1] D. C. White, H.H.Woodson.Electro Mechanical Energy Conversion [C]. Wiley, New York, 1959.

[2] Li Zhijian. Research on Phase Current Optimal Control Method for Symmetrical Six-Phase Motor Drive System [D]. University of Electronic Science and Technology of China, 2024.

[3] PrietoJ, RiverosJA, BogadoB, etal. Electric propulsion technology based in predictive direct torque control and asymmetrical dual three-phase drives[C].International IEEE Conference on Intelligent Transportation Systems.IEEE, 2010: 397-402.

[4] Oleschuk V,Ermuratskii V,Barrero F.Six-phase motor drive with variables witching frequencies and voltage synchronization of inverters[C]. International Conference on Electrical Drives and Power Electronics.IEEE,2015:69-75.

[5] Gonzalez-Prieto I, Duran M J, Barrero F, et al.Impact of Postfault Flux Adaptationon Six-Phase Induction Motor Drives With Parallel Converters[J].IEEE Transactions on Power Electronics, 2016, 32(1):515-528.

[6] Guzman H, Duran M J.Barrero F,et al.Speed Control of Five-Phase Induction Motors With Integrated Open-Phase Fault Operation Using Model-Based Predictive Current Control Techniques [J]. IEEE Transactions on Industrial Electronics, 2014, 61(9) : 4474-4484.